Journal of Nuclear Materials 400 (2010) 183–188

Contents lists available at ScienceDirect

Journal of Nuclear Materials

journal homepage: www.elsevier.com/locate/jnucmat

Phase studies in the UO_2–Gd_2O_3 system

M. Durazzo [a,*], F.B.V. Oliveira [a], E.F. Urano de Carvalho [a], H.G. Riella [b]

[a] Nuclear Energy Research Institute, IPEN-CNEN/SP, São Paulo, Brazil
[b] Chemical Engineering Department, Santa Catarina Federal University, Florianópolis, Brazil

ARTICLE INFO

Article history:
Received 5 February 2009
Accepted 1 March 2010

ABSTRACT

The incorporation of gadolinium directly into nuclear fuel is important regarding reactivity compensation, which enables longer fuel cycles. The incorporation of Gd_2O_3 powder directly into the UO_2 powder by dry mechanical blending is the most attractive process, because of its simplicity. Nevertheless, processing by this method leads to difficulties while obtaining sintered pellets with the minimum required density. This is due to the bad sintering behavior of the UO_2–Gd_2O_3 mixed fuel, which shows a blockage in the sintering process that hinder the densification process. Minimal information exists regarding the possible mechanisms for this blockage and this is restricted to the hypothesis based on the formation of a low diffusivity Gd rich $(U,Gd)O_2$ phase. The objective of this investigation was to study the phase formation in this system, thus contributing to clarifying the causes of the blockage. Experimental evidence indicated the existence of phases in the $(U,Gd)O_2$ system that revealed structures different from the fluorite-type UO_2 structure. These phases appear to be isostructural to the phases observed in the rare earth-oxygen system.

1. Introduction

The need to improve reactor performance through longer cycle lengths or improved fuel use has been apparent since the beginning of commercial nuclear power generation. Among several modifications introduced as a consequence, the initial fuel enrichment has been increased, which means that the additional amount of fissile material (^{235}U) in the reactor core has to be compensated by the introduction of additional neutron absorber material. The use of a burnable poison in nuclear reactors provides the necessary negative moderator reactivity coefficient at the beginning of core life and helps shape core power distributions [1]. From a nuclear viewpoint, gadolinia is an excellent burnable poison, possessing a high neutron absorption cross-section coupled to a burn up rate that, if properly designed, can closely match ^{235}U depletion, minimizing the reactivity penalty at end-of-cycle (EOC) [2,3]. The implantation of UO_2–Gd_2O_3 poisoned fuel in Brazil has been proposed according to the future requirements established for the Angra II nuclear power plant.

From the different methods for conversion of UF_6 to ceramic grade UO_2 in industrial scale [4], the Ammonium Uranyl Carbonate (AUC) process [5] is the most attractive due to the smallest number of process steps involved. In the AUC process, the Gd_2O_3 powder is incorporated into the UO_2 powder by the dry mechanical blending method. Next, the mixed UO_2 and Gd_2O_3 powder is directly pressed into pellet form, with no co-milling, prepressing and granulating steps [6,7].

Nevertheless, the incorporation of Gd_2O_3 powder into the AUC-derived UO_2 powder by the most attractive commercial method of dry mechanical blending leads to difficulties while obtaining sintered UO_2–Gd_2O_3 pellets with the minimum required density [7,8], due to the deleterious effect of the Gd_2O_3 on the traditional UO_2 sintering behavior. Several studies have investigated the sintering of UO_2–Gd_2O_3 mixed oxides, several of them indicated difficulties in sintering fuel pellets with the minimal specified density, of around 94% of the theoretical density. The sintering curves available in the literature show that the lower sintered densities are due to the abnormal sintering behavior of the UO_2–Gd_2O_3 fuel, compared to the sintering behavior of the traditional UO_2 fuel. Dilatometric analyses show that at temperatures around 1100–1400 °C, the shrinkage of the UO_2–Gd_2O_3 pellets is delayed, the sintering rate decreases and densification shifts to higher temperatures [7,9,10]. This phenomenon is what we denominated the "sintering blockage" and was confirmed in a previous work [11], when Gd_2O_3 powder was added to AUC-derived UO_2 powder by the dry mechanical blending route. Fig. 1 shows the typical sintering curve revealing this abnormal sintering behavior.

Manzel and Dörr [7] attributed the low densities observed in sintering UO_2–Gd_2O_3 pellets to the formation of a solid solution simultaneously with the densification process. During sintering, the diffusion processes lead not only to densification but also to the formation of solid solutions. The interdiffusion processes decrease the sintering rate and shift densification to higher

* Corresponding author. Address: Av. Prof. Lineu Prestes, 2242, Cidade Universitária, CEP 05508-000, São Paulo, SP, Brazil. Tel.: +55 11 31339196; fax: +55 11 31339280.
E-mail address: mdurazzo@ipen.br (M. Durazzo).

0022-3115/$ - see front matter © 2010 Elsevier B.V. All rights reserved.
doi:10.1016/j.jnucmat.2010.03.001

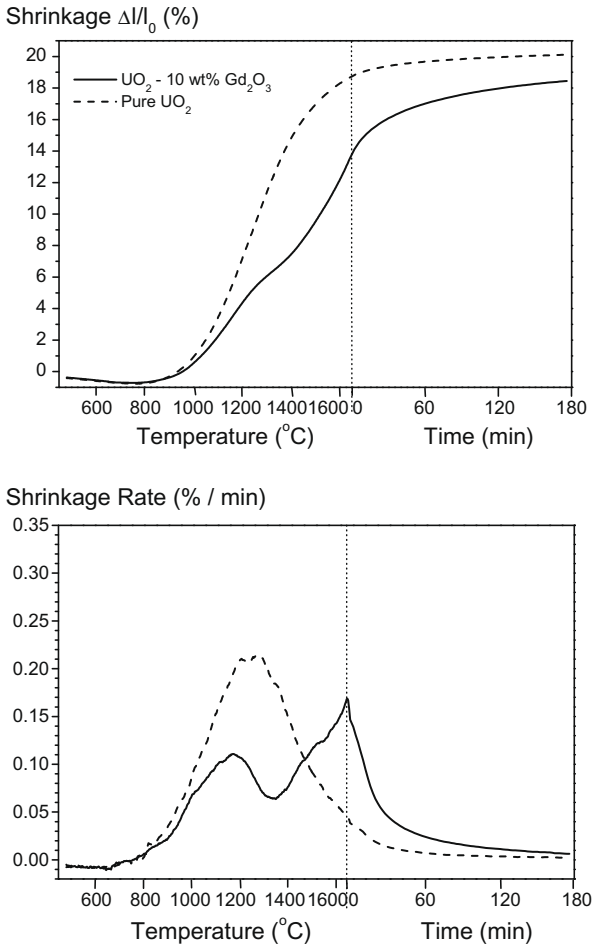

Fig. 1. Effect of Gd_2O_3 on the sintering behavior of UO_2–Gd_2O_3 fuel pellets (dry mechanical blending/5 °C/min).

temperatures. Assmann et al. [8] complemented this proposition by verifying that the diffusion coefficients in the UO_2–Gd_2O_3 system show a complex dependence on the U:Gd:O ratio in the oxide phases formed. Peehs et al. [12] detected the presence of the $(U_{0.5}Gd_{0.5})O_2$ phase in sintered UO_2–Gd_2O_3 pellets; however, their report did not discuss the possible participation of that phase in the sintering blockage mechanism. In all these studies, the samples were prepared by the dry mechanical blending method, which used UO_2 powder derived from the AUC process.

Considering that sintering blockage occurs during the solid solution formation, that the diffusion coefficient depends on the oxide phases formed and that a $(U_{0.5}Gd_{0.5})O_2$ phase has been verified, it can be inferred that the cause for the sintering blockage in the UO_2–Gd_2O_3 system is related to the formation of low diffusivity phases during the sintering process, which reduce densification and lead to low sintered densities. In this work, the existence of phases with low cation diffusivity in the $(U,Gd)O_2$ system were investigated, as these could confirm the explanation presented above. From this point onward, this proposed mechanism will be referred as the "diffusion barrier hypothesis".

2. Phase studies

The Ammonium Diuranate (ADU) coprecipitation method is widely used for UO_2–Gd_2O_3 powder and pellet preparation with a high degree of gadolinium homogeneity (solid solution). This method is mostly used in laboratories to produce homogeneous pellets for measuring the cell constants and thermal properties of $(U,Gd)O_2$ solid solutions [13–15]. Thus, this method was selected for sample preparation.

2.1. Experimental

The samples were prepared by coprecipitation from the ADU process, starting from mixed nitrate solutions. The UO_2–Gd_2O_3 mixed powders were fabricated with Gd_2O_3 content ranging from 0 to 100 wt.%. The 99.9% pure gadolinium oxide was supplied by Ventron Alfa Produkte. UO_2 powder was obtained from uranium hexafluoride via AUC conversion. The aqueous solutions of uranyl nitrate and gadolinium nitrate were prepared by dissolving UO_2 and Gd_2O_3 powders with 7N nitric acid solution. The uranyl and gadolinium nitrate solutions were thoroughly blended together in varying proportions up to 100 wt.% Gd_2O_3. The ADU was precipitated by adding 13 M NH_4OH solution (4 ml/min) to the $UO_2(NO_3)_2$/$Gd(NO_3)_3$ solutions at 60 °C. The final pH value was adjusted to pH 9. Samples were stirred with a glass rod while adding solution. The precipitates were vacuum filtered and dried in an oven at 80 °C for 24 h. The dried precipitates were reduced to uranium–gadolinium oxide in a tubular furnace at 650 °C under hydrogen atmosphere.

The mixed oxide powders were pressed into pellets ranging from 250 to 400 MPa, in order to obtain green densities of around 50% of the theoretical density. Before pressing, the powders were granulated to achieve the required green density. The granules were prepared by triturating manually the powders that were pre-pressed to 50% theoretical density. The green pellets were sintered in a hydrogen atmosphere at 1650 °C for 3 h. The sintered densities were determined by measuring the weight of the samples immersed in xylol (Archimedes principle).

2.2. Results and discussion

The variation in the sintered densities as a function of the molar fraction of gadolinium in the samples clearly demonstrated that a range of gadolinium concentrations exist for which the sintered densities unequivocally decrease with increasing Gd content (Fig. 2). An initial increase in the sintered density reached saturation, beginning with the composition $(U_{0.9}Gd_{0.1})O_2$, and a high densification level was maintained up to the composition $(U_{0.5}Gd_{0.5})O_2$. For this gadolinium concentration range the sintered densities remain very high, about 98–99% of the theoretical

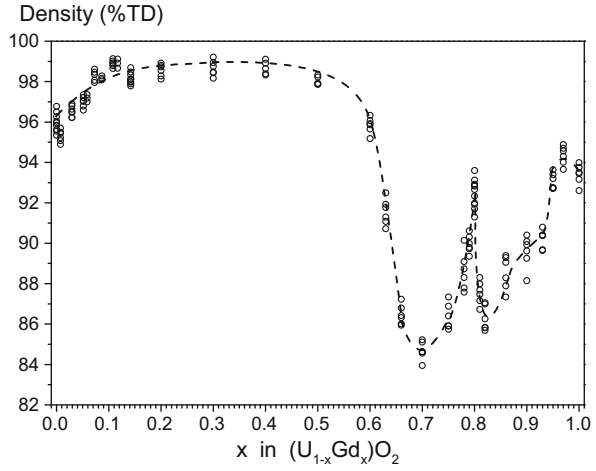

Fig. 2. Effect of the gadolinium concentration on the sintered density of $(U,Gd)O_2$ pellets prepared by coprecipitation (solid solution).

density. These high sintered densities can be explained according to the model proposed by Ho and Radford [16], in which the presence of Gd^{3+} ions causes an increase in the cation diffusivity and, therefore, an increase in the sinterability of the UO_2.

When the number of Gd atoms surpassed the number of U atoms (Gd > 0.5), the sintered densities decreased drastically, reaching a minimum value for the composition $(U_{0.3}Gd_{0.7})O_2$. A further increase in the molar fraction of gadolinium increased the sinterability of the $(U,Gd)O_2$ system again, until it reached a maximum value for the composition $(U_{0.2}Gd_{0.8})O_2$, for which densities of about 93% of the theoretical density were obtained. After this densification peak, a second decrease in sinterability occurred. Another minimum was observed for the composition $(U_{0.18}Gd_{0.82})O_2$, when the densification level rose to the typical density achieved when sintering pure Gd_2O_3 pellets (94% of the theoretical density).

It is interesting to note the behavior of the curve presented in Fig. 2 between the compositions $(U_{0.3}Gd_{0.7})O_2$ and $(U_{0.18}Gd_{0.82})O_2$, where a peak in the sintered densities was observed. This behavior was confirmed through repetitions in sintering tests for the composition $(U_{0.2}Gd_{0.8})O_2$ and by sintering the intermediate compositions between Gd = 0.7 and Gd = 0.9.

The UO_2–Gd_2O_3 sintered pellets were milled and analyzed by X-ray diffraction. The lattice parameter of $(U,Gd)O_2$ were determined with base on the diffractograms by analysing the 2θ position for the more intense (1 1 1) planes. Fig. 3 presents the variation in the lattice parameter as a function of the molar fraction of gadolinium in the samples. A linear decrease in the lattice parameter occurred for compositions up to $(U_{0.5}Gd_{0.5})O_2$, in agreement with Vegard's law. This observation indicated the presence of a single-phase with a fluorite-type structure, with Gd^{3+} ions substituting U^{4+} (solid solution). Despite the inaccuracy of this data, a good adjustment for a line can be observed.

When the molar fraction of gadolinium surpassed the value 0.5, the behavior of the lattice parameter of the fluorite structure was no longer linear, which indicated the end of the single-phase field. For compositions between $(U_{0.25}Gd_{0.75})O_2$ and $(U_{0.10}Gd_{0.90})O_2$, the diffractograms indicated the presence of the body-centered cubic structure, when a tendency toward a linear decrease in the lattice parameter as a function of the molar fraction of gadolinium was also observed. However, in this case, it was not possible to affirm that Vegard's law was obeyed, since bad adjustment was obtained for linear regression from the experimental data. This observation suggests the existence of two or more phases in this composition range. An attempt to fit a straight line to the data is illustrated in Fig. 3.

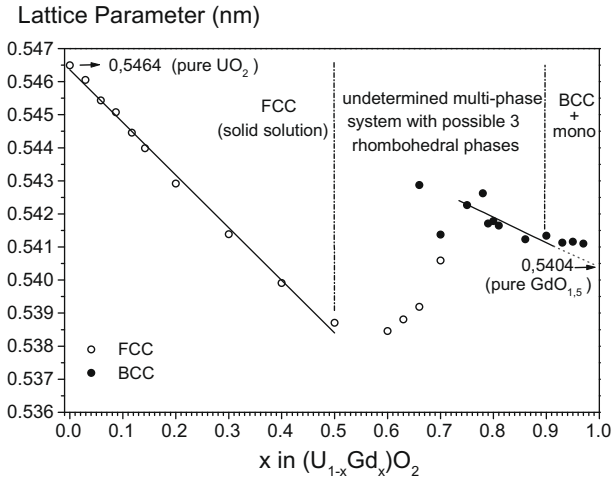

Fig. 3. Variation in the lattice parameter according to dissolved gadolinium content.

In the intermediate range of composition between $(U_{0.5}Gd_{0.5})O_2$ and $(U_{0.25}Gd_{0.75})O_2$ it is not possible to determine that simple coexistence between the FCC and BCC phases occurred, since the lattice parameter was not constant for either of the two structures. For compositions between $(U_{0.25}Gd_{0.75})O_2$ and $(U_{0.1}Gd_{0.9})O_2$ it is also not possible to determine that the system is a single-phase involving the BCC structure, since it is not possible to determine that Vegard's law was obeyed. Therefore, in this extensive composition range, where the molar fraction of gadolinium varies from 0.5 to 0.9, the results presented in Fig. 3 indicate the existence of one or more phases different from the FCC fluorite structure of UO_2 and BCC of Gd_2O_3. For compositions over $(U_{0.10}Gd_{0.90})O_2$ the coexistence of the C and B forms of Gd_2O_3 was verified, involving BCC and monoclinic structures, respectively.

Aitken et al. [17] observed a phase with a rhombohedral structure in the U–Y–O system, with composition varying over a wide range of yttrium concentrations, from 51 to 86 mol%; this phase was designated RI. A second phase, designated RII, was observed in this system, also showing a rhombohedral structure with composition varying between 68 and 75 mol% yttrium. These two rhombohedral phases were also observed in the U–La–O system, together with a third rhombohedral phase, designated RIII, which was detected in the concentration range varying from 55 to 67 mol% of lanthanum [18].

These rhombohedral phases were also observed in the compounds U–R–O (R = Nd, Sm, Eu, Ho, Er, Tm, Yb and Lu) and in the rare earth R–O system, where R = Ce, Pr and Tb, which can present valences +3 and +4. Kang and Eyring [19] observed that these rare earths exhibit a family of binary oxides where the valences +3 and +4 coexist, resulting in oxygen deficient fluorite related structures. Among these, the composition R_7O_{12} has the same rhombohedral structure observed in the U–Y–O system. In this report and in a subsequent study [20], the authors proposed the construction of crystalline structures of a group of compounds in the R–O system by assembling modules, which are unitary cells of the fluorite structure with oxygen vacancies in different positions in the unitary cell. Based on this mechanism, these researchers established and characterized 14 different phases in the R–O system. The R_7O_{12} phase is isostructural to the rhombohedral UGd_6O_{12} phase.

The experimental observation of the phases constructed based on the methodology proposed by Kang and Eyring, indicated that an extensive series of phases with structures based on the fluorite structure may exist, in which oxygen vacancies are distributed in different ways. This is an important conclusion, since phases that are isostructural to the phases observed by Kang and Eyring in the R–O system probably exist in the U–Gd–O system. The U^{4+} cation could be present in these structures substituting the R^{4+} cation. Moreover, the possibility that U^{5+} and U^{6+} cations also exist and the possibility of the occurrence of phases more complex than those already identified cannot be discarded.

Many researchers [13,21–23] agree that stoichiometry in the $(U,Gd)O_2$ system remains close to 2 up to a concentration of 40 mol% Gd_2O_3. A slight hypostoichiometry in this system for this Gd_2O_3 concentration range was also observed. Starting from 40 mol% Gd_2O_3, Beals and Handwerk [21] observed a consistent decrease in the O/M ratio in relation to the increase in the molar fraction of gadolinium, until the value of 1.5 was reached in the case of pure Gd_2O_3. According to the literature, when Gd^{3+} cations are incorporated into the fluorite structure, U^{4+} cations may be oxidized for charge compensation. According to Ohmichi et al. [23], the formation of a small proportion of oxygen vacancies may also occur, probably randomly distributed in the crystal lattice of the solid solution, which is verified by the hypostoichiometry. This mechanism, which conforms to model 3 proposed by Ho and

Radford [16], could be considered valid for Gd_2O_3 concentrations up to 50 mol%.

Above 50 mol% in Gd_2O_3, a systematic formation of oxygen vacancies for charge compensation occurred, as is indicated in the literature [21]. When the number of oxygen vacancies reaches a critical value, the oxygen vacancies rearrange to form new phases that would be isostructural to those observed and modeled by Kang and Eyring in the R–O system, as discussed previously. The rhombohedral phase is probably one of them. Thus, the variation in the lattice parameter as a function of the molar fraction of gadolinium ceases to satisfy Vegard's law. With the continuous increase in the number of oxygen vacancies, the crystal structure develops until obtaining the BCC structure of Gd_2O_3, where 16 oxygen vacancies are present. If the straight line that represents the lattice parameter variation for the composition range of $x = 0.75$–0.9 is extrapolated, it intercepts the ordinate axis at the value 0.5404 nm for $x = 1$ ($GdO_{1.5}$), which is very close to the X-ray diffraction standard value of 1.0813 nm for the Gd_2O_3 unitary cell, or 0.5407 nm for the pseudo fluorite cell of the $GdO_{1.5}$.

The onset of diminished sinterability in the UO_2–Gd_2O_3 system corresponds to the end of the monophase area in the system, with the fluorite structure, for the composition $(U_{0.5}Gd_{0.5})O_2$ (see Figs. 2 and 3). This also corresponds to the onset of the systematic formation of oxygen vacancies, verified by the decrease in the O/M ratio, which was almost constant until this composition, as indicated in the literature [21]. Although new $(U,Gd)O_2$ phases were not observed directly in this study, the results support the proposition that the onset of the systematic oxygen vacancies formation facilitates the formation of new $(U,Gd)O_2$ phases in the system, which are different from the fluorite phase. One very probable phase is the rhombohedral phase observed in the U–Y–O system, which should be isostructural to that observed in the rare earth oxides CeO_{2-x}, PrO_{2-x} and TbO_{2-x}. Such a complex phase structure would be responsible for a decrease in the cation diffusivity of the system, leading to diminished sinterability. The presence of some phase with good diffusivity (not detected directly in this work) could be responsible for the form of the curve presented in Fig. 2, which revealed good sinterability for the composition $(U_{0.2}Gd_{0.8})O_2$.

The experimental results presented in Fig. 2 provide the basis for the proposed diffusion barrier hypothesis, since molar fractions of gadolinium higher than 0.5 resulted in very low sintered densities. The occurrence of phases different from fluorite for molar fractions of gadolinium higher than 0.5 was also observed, which could explain the decrease in sinterability. However, nothing can be determined regarding the dependence of the interdiffusion coefficient in the UO_2–Gd_2O_3 system on the gadolinium concentration, which is ultimately what determines the sinterability of the system. Aimed at complementing the basis of the diffusion barrier hypothesis, an interdiffusion study concerning the UO_2–Gd_2O_3 system was realized; the results are presented and discussed in the following section.

3. Interdiffusion studies

The interdiffusion studies were conducted by determining the gadolinium profile concentration (penetration curves) in a sintered UO_2/Gd_2O_3 couple. The interdiffusion coefficient was determined as a function of the molar fraction of gadolinium by applying the Matano–Boltzman method.

3.1. Experimental

The UO_2/Gd_2O_3 couple was prepared by simultaneously compacting both the UO_2 and Gd_2O_3 powders. Initially, the die cavity was filled with Gd_2O_3 powder, which was precompacted at low pressure. Next, the UO_2 powder was introduced in the die cavity and the couple was compacted to form a solid body with a density of approximately 50% of the theoretical density, which was calculated considering the average between the UO_2 and Gd_2O_3 theoretical densities. The pressure for precompaction of the Gd_2O_3 powder was very low, below the detection limit of the press. High precompaction pressures invariably led to low mechanical resistance in the UO_2/Gd_2O_3 interface. The couple was sintered at 1650 °C for 3 h. The heating rate was 5 °C/min and the sintering atmosphere was pure hydrogen. The couple obtained after sintering presented good mechanical resistance at the interface, which made it possible to make a longitudinal cut perpendicular to the interface. The surface of the sample was prepared through conventional metallographic techniques.

Initially, qualitative analysis was conducted on the polished surface, where the appearance of the UO_2/Gd_2O_3 interface was revealed through scanning electron microscopy and the general form of the concentration profile was determined through qualitative analysis (EDS) of the gadolinium concentration over a line perpendicular to the interface. Once observation of the interface was completed, three areas were selected where continuity between the pure UO_2 and pure Gd_2O_3 phases were observed. In these areas, quantitative analyses were realized for the gadolinium concentration through WDS in points spaced at 0.5 μm from each other. The precision in the determination of the gadolinium concentration was estimated to be 0.1%. From the penetration curves, the interdiffusion coefficient was determined through graphic integration applying the Matano–Boltzmann method.

3.2. Results and discussion

Fig. 4 presents an electronic micrography illustrating the UO_2/Gd_2O_3 interface. In general, the presence of a void was observed between the phases, between 1 and 3 μm wide. The uranium and gadolinium concentrations were determined along the line indicated in Fig. 4. The concentration profiles indicated interpenetration of approximately 16 μm after sintering for 3 h at 1650 °C. The gadolinium penetration into the UO_2 phase was notably greater than the uranium penetration into the Gd_2O_3 phase, greater than 2/3 of the total interpenetration distance.

An inspection was conducted along the interface, aimed at selecting areas with good continuity between the UO_2 and Gd_2O_3 phases, where the width of the void was minimal. Three areas were selected, which presented good continuity between the phases. In these areas, quantitative analyses were performed for gadolinium

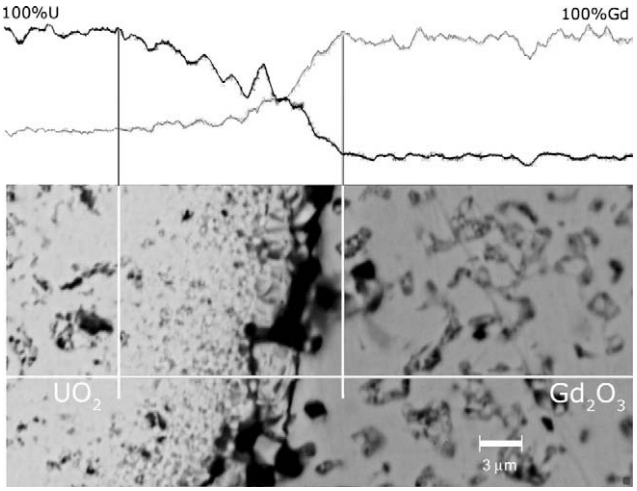

Fig. 4. Scanning electron micrograph illustrating the UO_2/Gd_2O_3 interface.

concentration determination at points spaced 0.5 μm along a line normal to the UO_2/Gd_2O_3 interface line. The experimental points are presented in Fig. 5 Once the penetration curve had been constructed, the interdiffusion coefficient in the UO_2–Gd_2O_3 system was calculated as a function of the molar fraction of gadolinium by applying the data analysis method proposed by Matano [24].

The Matano method is a graphic method for the solution of Fick's second law, given by the differential equation:

$$\frac{\partial c}{\partial t} = \frac{\partial}{\partial x}\left(D\frac{\partial c}{\partial x}\right) \tag{1}$$

where c is concentration, t is time and x is position.

This method was applied using the experimental penetration curve, which was derived from the experimental data presented in Fig. 5. Fig. 6 illustrates the applied methodology. As a first step, the areas below and above the penetration curve were integrated from $x = 0.25$ μm spaced elements, totalizing 56 elements in the total interpenetration distance of 14 μm. The intersection between the curves of cumulative area below and above the penetration curve determines the position of the Matano plane, which divides the integral of concentration in two equal parts. This position is taken as the new zero position, as indicated in Fig. 6. This construction satisfies the condition imposed by the method:

$$\int_0^1 x\ \partial c = 0 \tag{2}$$

Next, the integral of concentration from zero to the concentration for which the interdiffusion coefficient will be determined, is determined graphically together with the tangent of the penetration curve for that concentration. In Fig. 6, the methodology is presented for a generic concentration c.

Thus, the differential equation:

$$D = \frac{1}{2t}\frac{\partial x}{\partial c}\int_0^c x\ \partial c \tag{3}$$

is solved by calculating the area indicated in Fig. 6 and the value of the tangent of the curve for the concentration c:

$$D = \frac{1}{2t}\frac{1}{\text{tangent at } c}(\text{area from } c1 = 0 \text{ to } c) \tag{4}$$

In this work, the diffusion time was considered to be 3 h. The heating period up to the temperature test (1650 °C) was discarded.

The interdiffusion coefficient was calculated for 0 to 100 mol% of gadolinium and the results are presented in Fig. 7 The most important characteristic in this figure is the sudden decrease in the interdiffusion coefficient for gadolinium concentrations above 50 mol%. It is also interesting to observe the increase in the interdiffusion coefficient for gadolinium concentrations of about 80 mol%. These results show good agreement with those presented in Fig. 2 and directly confirm that the interdiffusion coefficient in the UO_2–Gd_2O_3 system decreases abruptly when the molar fraction of gadolinium is higher than 0.5, or when more than half of the cations present are Gd^{3+}. Despite the imprecision of the applied method, as verified by the considerable dispersion of the experimental data presented in Fig. 5, it is conclusive that UO_2–Gd_2O_3 sinterability decreased drastically starting from the composition $(U_{0.5}Gd_{0.5})O_2$, due to a sudden decrease in the interdiffusion coefficient of the system from that composition onward.

The results presented in Fig. 7 agree in many aspects with those obtained by other researchers. Loose et al. [25] studied interdiffusion in the UO_2–Gd_2O_3 system through pairs prepared starting from a precompacted Gd_2O_3 pellet positioned inside UO_2 powder, which were pressed simultaneously. Sintering was carried out under temperatures ranging from 1600 to 1900 °C for 4, 16 and 64 h. The penetration curves were obtained from autoradiographs impressed by alpha particles emitted by the samples. Nishida and Yuda [26] also studied interdiffusion in the UO_2–Gd_2O_3 system

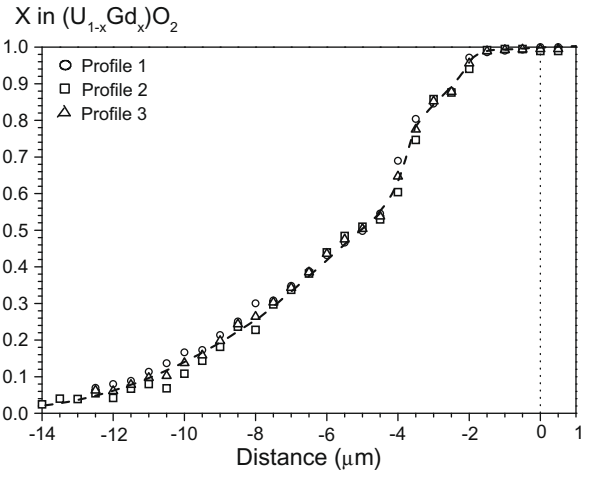

Fig. 5. Concentration profile across the UO_2/Gd_2O_3 interface.

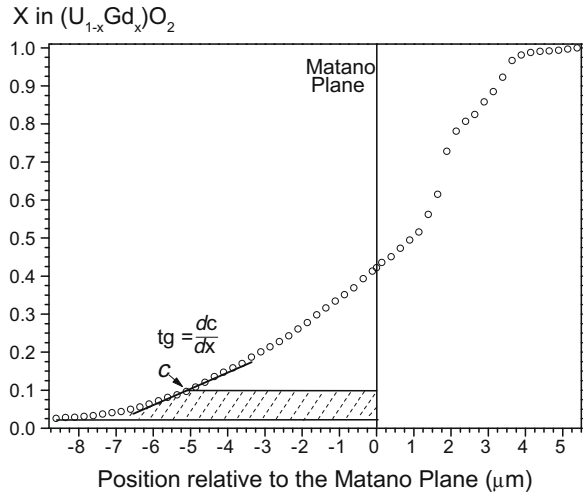

Fig. 6. Application of the Matano's methodology to the experimental penetration curve.

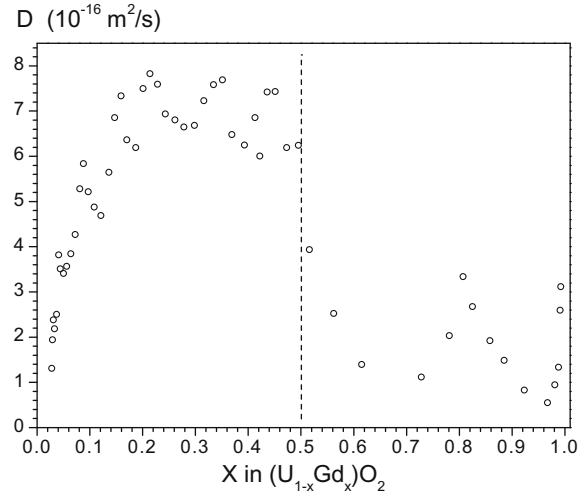

Fig. 7. Interdiffusion coefficient as a function of the molar fraction of gadolinium.

through pairs prepared in a similar way. In this case, sintering was carried out at 1700 and 1800 °C for 100 h and the concentrations were determined by EDS. The authors also obtained complex penetration curves, like those obtained in this work.

The penetration curve obtained by Loose et al. [25] in their sample sintered at 1900 °C for 64 h revealed a shape very similar to that obtained in this work based on the shape of the penetration curve, the authors concluded that phases other than the fluorite phase occurred. In contrast, the penetration curves obtained by Nishida and Yuda [26] are considerably different from the curve obtained in this work. The reason for this discrepancy is related to the large void observed by these researchers in the interface UO_2/Gd_2O_3, which was about 50 μm wide.

Unfortunately, in these two published works, the authors discarded the form of the penetration curves and assumed that the interdiffusion coefficient was independent of the gadolinium concentration. They calculated the effective interdiffusion coefficient. According their results, the interdiffusion coefficient in the UO_2–Gd_2O_3 system can be calculated from the expressions:

$$D = 3.3 \cdot 10^{-10} \exp(200,000(\mathrm{J/mol})/RT)(\mathrm{m^2/s})[25] \quad (5)$$

$$D = 1.0 \cdot 10^{-10} \exp(260,000(\mathrm{J/mol})/RT)(\mathrm{m^2/s})[26] \quad (6)$$

Starting from these expressions, the interdiffusion coefficients can be calculated considering the conditions adopted in this work, for 1650 °C and 3 h. The values 12.2. 10^{-16} m^2/s [25] and 0.9. 10^{-16} m^2/s [26] would be obtained. The value obtained considering the expression formulated by Loose et al. agrees reasonably well with the results obtained in this work; however, the value obtained by the expression determined by Nishida and Yuda can be considered low compared with the experimental results presented in Fig. 7. This conclusion can be inferred by the small interpenetration observed in the results obtained by these researchers compared to those obtained in this work. Nishida and Yuda obtained an interpenetration of 25 μm while sintering at 1700 °C for 100 h. In this work, under sintering conditions much less severe (3 h at 1650 °C), an interpenetration of 14 μm was obtained. This discrepancy can be explained by the large void (approx. 50 μm) that occurred at the UO_2/Gd_2O_3 interface in the samples prepared by Nishida and Yuda, as previously mentioned.

4. Conclusions

The presence of phases with crystalline structure different from the UO_2 fluorite structure was detected. These phases have low diffusivity and occur when the molar fraction of gadolinium surpasses the value of 0.5. The new phases could not be completely characterized in this work, but they are probably isostructural to the series of phases identified in the Ce–O, Pr–O and Tb–O systems. This experimental evidence supports the hypothesis most frequently proposed to explain the sintering behavior of UO_2–Gd_2O_3 fuel. The hypothesis is based on the formation of a diffusion barrier around the Gd_2O_3 agglomerates due to the formation of the gadolinium rich phases with low diffusivity. Further work is being developed to confirm this hypothesis.

Acknowledgments

The authors wish to express their gratitude to CTMSP (Navy Technological Center in São Paulo) for the permission to use its facilities. The authors also wish to thank the IAEA (International Atomic Energy Agency) for partially supporting this study.

References

[1] W. Böhm, H.D. Kiehlmann, A. Neufert, M. Peehs, Kerntechnik 50 (4) (1987) 234.
[2] E. Hellstrand, Trans. Am. Nucl. Soc. 40 (1982). 181.
[3] F.B. Skogen, L.A. Nielsen, R.G. Grummer, Trans. Am. Nucl. Soc. 40 (1982) 194.
[4] S.G. Brandberg, Nucl. Technol. 18 (1973) 177.
[5] H. Assmann, M. Becker, Trans. Am. Nucl. Soc. 31 (1979) 147.
[6] H. Assmann, W. Dörr, Mater. Sci. Monogr. 16 (1983) 707.
[7] R. Manzel, W. Dörr, Am. Ceram. Soc. Bull. 59 (6) (1980) 601.
[8] H. Assmann, M. Peehs, H. Roepenack, J. Nucl. Mater. 153 (1988) 115.
[9] K.W. Song, K.S. Kim, J.H. Yang, K.W. Kang, Y.H. Jung, J. Nucl. Mater. 288 (2001) 92.
[10] R. Yuda, K. Une, J. Nucl. Mater. 178 (1991) 195.
[11] M. Durazzo, H.G. Riella, Key Eng. Mater. 189–191 (2001) 60.
[12] M. Peehs, W. Dörr, G. Gradel, G. Maier, J. Nucl. Mater. 106 (1982) 221.
[13] S. Fukushima, T. Ohmichi, A. Maeda, H. Watanabe, J. Nucl. Mater. 105 (1982) 201.
[14] T. Wada, K. Noro, K. Tsukui, Behavior of UO_2–Gd_2O_3 Fuel, in: Proc. Int. Conf. on Nuclear Fuel Performance, 15–19 October, 1973, London, 1973, p. 63.1.
[15] C. Miyake, M. Kanamaru, S. Imoto, J. Nucl. Mater. 137 (1986) 256.
[16] S.M. Ho, K.C. Radford, Nucl. Technol. 73 (1973) 350.
[17] E.A. Aitken, S.F. Bartram, E.F. Juenke, Inorg. Chem. 3 (7) (1964) 959.
[18] K.A. Gschneider Jr., L. Eyring, Handbook on the Physics and Chemistry of Rare Earths. Non-metallic Compounds – I, vol. 3, Springer, US, 1979. pp. 444.
[19] Z.C. Kang, L. Eyring, J. Alloys Compd. 249 (1997) 206.
[20] Z.C. Kang, L. Eyring, J. Alloys Compd. 275–277 (1998) 30.
[21] R.J. Beals, J.H. Handwerk, J. Am. Ceram. Soc. 48 (5) (1965) 271.
[22] K. Une, M. Oguma, J. Nucl. Mater. 110 (1982) 215.
[23] T. Ohmichi, S. Fukushima, A. Maeda, H. Watanabe, J. Nucl. Mater. 102 (1981) 40.
[24] C. Matano, Jpn. J. Phys. 8 (3) (1933) 109.
[25] A. Loose, R. Ilic, V. Marinkovic, A. Trkov. Diffusion measurements in UO_2–Gd_2O_3, in: Proc. of an International Symposium on Improvements in Water Reactor Fuel Technology and Utilization, Vienna, IAEA-SM-288/36P, 1987, p. 578.
[26] T. Nishida, R. Yuda, Effect of particle size and oxygen potential on UO_2/Gd_2O_3 pellet sintering, advances in fuel pellet technology for improved performance at high burnup, in: Proc. of a Technical Committee Meeting, Vienna, October 28–November 01, 1996, IAEA-TECDOC—1036, 1998, p. 73.